Surface optical phonons as a probe of organic ligands on ZnO nanoparticles: An investigation using a dielectric continuum model and Raman spectrometry

P.-M. Chassaing, F. Demangeot, V. Paillard, A. Zwick, and N. Combe
Centre d'Elaboration de Matériaux et d'Etudes Structurales, CNRS UPR 8011, 29 rue Jeanne Marvig, 31055 Toulouse Cedex 4, France and Université Paul Sabatier, 118 Route de Narbonne, 31062 Toulouse Cedex 9, France

C. Pagès, M. L. Kahn, A. Maisonnat, and B. Chaudret
Laboratoire de Chimie de Coordination, CNRS UPR 8241, 205 Route de Narbonne, 31077 Toulouse Cedex 4, France
(Received 12 February 2008; published 23 April 2008)

Surface optical modes in cylindrical ZnO nanoparticles have been studied theoretically using a dielectric continuum model and experimentally by Raman spectrometry. Theoretically, both wave vector dispersion and outer medium dielectric constant effects have been investigated. Consequently, we attribute the intense peak at 490 cm^{-1} in the Raman experiment to a surface optical mode related to the top basis of the nanoparticles. We deduce that the bonding of long alkyl chain amines is likely related to the lateral surface of the nanoparticles.

DOI: 10.1103/PhysRevB.77.153306 PACS number(s): 68.35.Ja, 78.30.−j, 63.22.−m

INTRODUCTION

Reducing size of semiconductors to the nanometric range, electronic and mechanical properties are strongly modified compared to bulk due to an important surface and/or volume ratio, opening thus the way to create new materials.[1] Among modified vibrational properties, surface optical phonon (SOP), or interface optical phonon (IOP) (for nanostructures embedded in a solid matrix), becomes significant for quantum dots smaller than a few nanometers. For example, IOP in zinc-blende GaAs/AlAs planar heterostructures[2] has been observed by Raman spectroscopy. SOP or IOP is strongly conditioned by the shape of nanoparticles (NPs): in particular, the study of cylindrical objects (quantum dots and quantum well wires)[3–5] points out the existence of side surface optical (SSO) modes related to the cylindrical interface and top surface optical (TSO) modes related to the planar one.

In view of a widespread range of applications,[6,7] zinc oxide (ZnO) is one of the materials that is intensely studied: for instance, Fonoberov and Balandin theoretically investigated the polar optical phonons in ZnO NPs of spherical[8,9] and ellipsoidal[10] shapes, showing the influence on SOP of the dielectric constant of the outer medium.

SAMPLE PREPARATION AND EXPERIMENTAL SETUP

Objects studied here are synthesized by a one step wet chemistry method:[11] a solution of an organometallic precursor $[Zn(Cy)_2]$ is left in ambient air after the addition in the reaction media of ligands, which are long alkyl chain amines. The solvent evaporation remains a white powder identified as ZnO NPs shaped as straight prisms with hexagonal basis. Ten samples have been studied; we have chosen to report precise data and characterizations of five representative nano-objects. Morphological and ligand properties of these samples are listed in Table I.

Samples were studied by room temperature micro-Raman experiments performed with a XY Dilor spectrometer and were excited with a Kr^+ laser. It is known that ZnO NPs can be locally heated by laser beam beyond absorption (3.36 eV), leading to important shifts of vibrational mode frequencies.[12] We used a wavelength below absorption (647.1 nm, 1.92 eV) and low power excitation ($\leq$10 mW), ensuring our Raman spectra not skewed by heating of NPs.

Previous nuclear magnetic resonance[11] and photoluminescence[13] studies deal with the coordination of ligands on NPs from the synthesis. In this Brief Report, we use the sensitivity of SSO and TSO mode frequencies on surface environment in cylindrical objects to probe the presence of ligands on the NP surface. SSO and TSO modes in the approximation of a cylinder are theoretically calculated using a dielectric model and compared to experimental results. We conclude that ligands are located on the NP lateral surface, rather than on their top surfaces.

POLAR OPTICAL MODES IN AN INFINITELY LONG CYLINDER

Let us consider a cylindrical interface of radius a between wurtzite ZnO and an outer medium of dielectric constant ε_D. With Oz parallel to c axis of ZnO, the permittivity tensor of ZnO is given by

$$\varepsilon(\omega) = \varepsilon_\perp(\omega)\begin{pmatrix} 1 & 0 & 0 \\ 0 & 1 & 0 \\ 0 & 0 & g(\omega) \end{pmatrix}, \quad (1)$$

where $g(\omega)=\varepsilon_\parallel(\omega)/\varepsilon_\perp(\omega)$. Components of $\varepsilon(\omega)$ are given by Loudon's uniaxial crystal model:[14] $\varepsilon_\perp(\omega)=\varepsilon_\perp^\infty(\omega^2-\omega_{\perp,LO}^2/\omega^2-\omega_{\perp,TO}^2)$, $\varepsilon_\parallel(\omega)=\varepsilon_\parallel^\infty(\omega^2-\omega_{\parallel,LO}^2/\omega^2-\omega_{\parallel,TO}^2)$, where $\varepsilon_\perp^\infty$ and $\varepsilon_\perp^\parallel$ are, respectively, the perpendicular and parallel to c axis high frequency dielectric constants, and $\omega_{\perp,LO}$, $\omega_{\perp,TO}$, $\omega_{\parallel,LO}$, and $\omega_{\parallel,TO}$ are the zone center frequencies of E_1(LO), E_1(TO), A_1(LO), and A_1(TO) symmetry modes, respectively. Numerical values of these parameters were taken from Refs. 7 and 15. Using cylindrical coordinates, we consider the following potential: $V(r,\theta,z)=f(r)\cos(m\theta)\exp(iq_z z)$. The symmetry of revolution around Oz axis imposes m to be an integer, and the dependency of the potential with respect to z corresponds to a plane wave propagating along Oz axis with

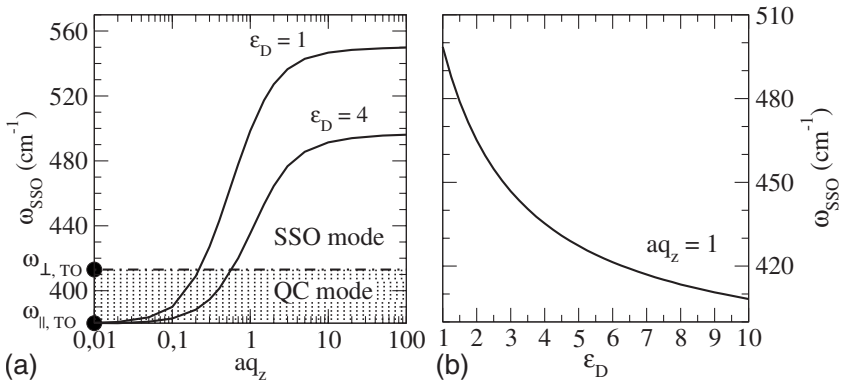

FIG. 1. Dispersion of QC/SSO modes with respect to aq_z (left) and ε_D (right).

the real wave vector q_z. Here, V satisfying the Maxwell–Gauss equation $\nabla[-\varepsilon(\omega)\nabla V]=0$ and f is equal to a linear combination of the modified Bessel functions of the first I_m and second kind K_m if $g(\omega)\geq 0$. Given that I_m (K_m) diverges for $r\to\infty$ $(r\to 0)$, the potential reads

$$V(r,\theta,z)=\cos(m\theta)\exp(iq_z z)\begin{cases} V_0^{in} I_m(iq_r r) & \text{for } r\leq a \\ V_0^{ext} K_m(q_z r) & \text{for } r\geq a, \end{cases} \tag{2}$$

where q_z and q_r inside the cylinder are related to

$$\varepsilon_\perp(\omega)q_r^2+\varepsilon_\parallel(\omega)q_z^2=0 \tag{3}$$

and where V_0^{in} and V_0^{ext} are arbitrary constants. To ensure the continuity of both V and the tangential electric field at the surface, we choose V_0^{in} and V_0^{ext} as $V_0^{in}=1/I_m(iq_r a)$ and $V_0^{ext}=1/K_m(q_z a)$. Equation (2) actually considers a SSO mode providing $g(\omega)\geq 0$ (q_r purely imaginary). Note that Eq. (2) also describes a quasiconfined (QC) mode if q_r is real, i.e., $g(\omega)\leq 0$.

In the following, we focus on polar optical modes without angular dependency $(m=0)$, which are likely observable in the Raman spectra because of their high symmetry. Writing the continuity of $\mathbf{D}_\perp$ at the surface, frequencies of polar optical modes are solutions of

$$\varepsilon_\perp(\omega)\sqrt{g(\omega)}+\varepsilon_D\frac{I_0(iq_r a)K_1(q_z a)}{I_1(iq_r a)K_0(q_z a)}=0. \tag{4}$$

By neglecting the anisotropy of ZnO $[g(\omega)=1]$, Eq. (4) reduces to Eq. (9) of Ref. 5 in the case of zinc-blende structure.

TABLE I. Characteristics of five samples under study. The aspect ratio is defined as the height of the NP divided by its diameter.

Sample	Diameter (nm)/ aspect ratio	Ligand	ε_{ligand}
1	2.1/1	Butylamine	5.0
2	6.8/1	Heptylamine	3.6
3	4.1/1	Octylamine	3.1
4	4.4/1	None (annealed NP)	
5	8.8/2.2	Octylamine	3.1

For $q_z\to 0$, solution of Eq. (3) gives $\omega(aq_z=0)=\omega_{\parallel,TO}$, and for $q_z\to\infty$, Eq. (4) leads to $\omega\to\omega_{SSO\infty}$ solution of

$$\sqrt{\varepsilon_\perp(\omega_{SSO\infty})\varepsilon_\parallel(\omega_{SSO\infty})}+\varepsilon_D=0. \tag{5}$$

As a consequence, solutions of Eq. (4) are in the range $[\omega_{\parallel,TO};\omega_{SSO\infty}]$. Note that $\omega_{SSO\infty}$ is greater than $\omega_{\perp,TO}$ no matter the value of ε_D. Thus, there is a cutoff value of $aq_{z,th}$ for which $\omega_{SSO}(aq_{z,th})=\omega_{\perp,TO}$. Only solutions for which $g(\omega)\geq 0$ $(\omega\in[\omega_{\perp,TO};\omega_{\parallel,LO}])$ describe a SSO mode. Below $aq_{z,th}$, the polar optical mode is no longer a surface mode but becomes QC $(\omega\in[\omega_{\parallel,TO};\omega_{\perp,TO}])$. This particularity has already been pointed out for GaN-AlN quantum well wire.[3] The above analytical discussion is illustrated by the curves presented in Fig. 1 obtained by numerical resolution of Eq. (4). In Fig. 1(a), we plot both curves for $\varepsilon_D=1$ (interface with the air) and $\varepsilon_D=4.0$, which is in the range of values under consideration for our samples (see Table I). QC mode region is labeled with a dotted background. In Fig. 1(b), $q_z=1/a$, which is in order of magnitude, the first nonzero wave vector activated due to axial confinement, considering a NP of aspect ratio of unity.

Figure 1(b) shows that SSO modes are strongly dispersive regarding the dielectric constant of the outer medium. Especially, looking in the range $\varepsilon_D\in[3,5]$, consistently with values reported in Table I, SSO mode frequencies shift by about 20 cm^{-1}.

TOP SURFACE OPTICAL MODES IN AN INFINITELY FLAT DISK

Let us now consider an infinitely flat disk (thickness l) of wurtzite ZnO bathing in an outer medium (dielectric constant ε_D'). We consider the following potential: $V(r,\theta,z)=J_m(q_r r)\cos(m\theta)h(z)$, where q_r is the real wave vector characterizing the propagation along the radial direction and J_m the Bessel function of the first kind. According to the Maxwell–Gauss equation, h is a linear combination of cosh and sinh unctions, respectively, corresponding to symmetric and antisymmetric modes with respect to $z=0$ plane. First, let us consider the case of a symmetric mode. The electrostatic potential has the following expression:

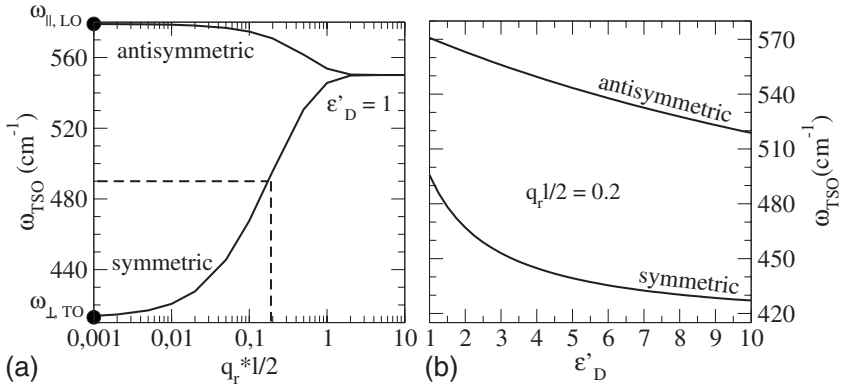

FIG. 2. Dispersion of TSO modes with respect to $q_r l/2$ (left) and ε'_D (right).

$$V(r,\theta,z) = J_m(q_r r)\cos(m\theta) \times \begin{cases} \cosh\left(\frac{q_r z}{\sqrt{g(\omega)}}\right) \Big/ \cosh\left(\frac{q_r l}{2\sqrt{g(\omega)}}\right) & \text{for } |z| \le \frac{l}{2} \\ \exp\left[q_r\left(\frac{l}{2} - |z|\right)\right] & \text{for } |z| \ge \frac{l}{2}. \end{cases} \quad (6)$$

Providing $g(\omega) > 0$, Eq. (6) describes a TSO mode, i.e., vanishing along the axial direction and propagating along the radial one. We find symmetric TSO mode frequencies ω^s_{TSO} by formulating the continuity $\mathbf{D}_\perp$ at $z = \pm l/2$, which leads to the following equation:

$$\tanh\left(\frac{q_r l}{2\sqrt{g(\omega)}}\right) + \varepsilon'_D \frac{\sqrt{g(\omega)}}{\varepsilon_\parallel(\omega)} = 0. \quad (7)$$

Similarly, antisymmetric TSO mode frequencies ω^{as}_{TSO} are solutions of

$$\coth\left(\frac{q_r l}{2\sqrt{g(\omega)}}\right) + \varepsilon'_D \frac{\sqrt{g(\omega)}}{\varepsilon_\parallel(\omega)} = 0. \quad (8)$$

Considering isotropic zinc-blende ZnO, Eqs. (7) and (8) reduce to equations (1a) and (1b) of Ref. 16, respectively. Figure 2(a) reports the frequencies of the symmetric and antisymmetric modes as a function of $q_r l/2$, with $\varepsilon'_D = 1$, i.e., in the case of an interface between ZnO and the air. Figure 2(b) reports the same quantity as a function of ε'_D with $q_r l/2 = 0.2$, which corresponds to the value deduced from our experiments as described further. For both symmetric or antisymmetric TSO mode, ω_{TSO} is in the range $[\omega_{\perp,TO}, \omega_{\parallel,LO}]$ for which $g(\omega)$ is always positive. Thus, unlike SSO modes, modes described in Eq. (6) never become QC into the NP. Such a behavior is not only due to structural anisotropy of wurtzite structure but also to the relative orientation of the surface normal vector and the wurtzite structure c axis. This last argument is also relevant to explain why polar optical modes can switch from SSO mode to QC mode. Another point is that for $q_r l/2 \to +\infty$, TSO modes tend to the value of ω_{SSO^∞} defined in Eq. (5). Thus, the surface curvature (cylindrical or planar) as well as the surface orientation do not have an effect on very short wavelength surface mode frequencies, in which lattice vibrations are located near the surface.

Moreover, it can be seen from Fig. 2(b) that both symmetric and antisymmetric TSO modes exhibit, as SSO modes, a strong dispersion with respect to the dielectric constant of the outer medium. Looking in the same range $\varepsilon_D \in [3,5]$ as before, TSO mode frequencies are redshifted by 12 cm^{-1} approximately.

COMPARISON BETWEEN CALCULATIONS AND EXPERIMENTS

Spectra of samples under study are presented in Fig. 3. The discussion concerning the E_2 mode frequency can be found in Ref. 17. As already discussed in Ref. 17 the intense peak located at 490 cm^{-1} on spectra is attributed to a SOP. In the following discussion, we address the following question: Is this mode related to lateral or top surfaces of NPs?

A key point is that no frequency shift of this peak is observed in all spectra in Fig. 3, although the dielectric constant of the outer medium is in the range between 3.1 and 5.0

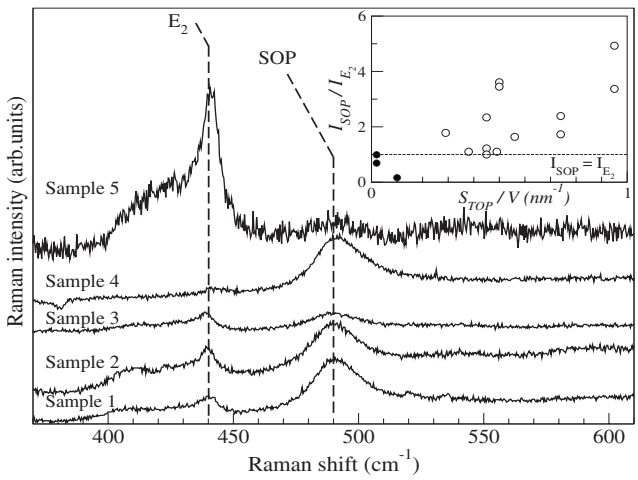

FIG. 3. Raman spectra of samples 1–5 (see Table I). Intensity of spectrum of sample 5 was multiplied by 6 compared to other spectra. Inset: plot of I_{SOP}/I_{E_2} (see text) versus S_{TOP}/V for all studied samples. Nanorods and NPs are denoted by filled and open circles, respectively.

according to Table I. Let us remind that our calculations predict downshifts of 20 cm^{-1} in the case of SSO modes and 12 cm^{-1} in the case of TSO modes. We conclude that the observed surface mode involves a surface free of ligands ($\varepsilon'_D=1$). According to our calculations [Figs. 1(b) and 2(b)], we could assign this surface mode to a SSO mode or a symmetric TSO mode. Considering intensities on the Raman spectra allows us to settle the issue: for all studied samples, we plotted the ratio of SOP mode intensity normalized by the E_2 mode intensity versus the top surfaces per volume ratio (see the inset of Fig. 3). Normalizing to the E_2 mode intensity makes it possible to compare SOP intensities of nanorods with those of NPs. The global trend revealed by the inset indicates that the SOP intensity increases with the top surfaces per volume ratio. This point is compatible with an observation of a symmetric TSO mode.

As an immediate consequence, no ligands are coordinated to the NP top surfaces. They should be mainly located on the NP lateral surface. Consequently, this proves that SOPs are sensitive probes in the presence of organic ligands on NPs. Results of the calculation in Fig. 2(a) show that the observed TSO mode has a wave vector $q_r=0.4/l$ [see dotted lines in Fig. 2(a)], i.e., $q_r=0.02-0.2$ nm^{-1} according to the range of heights of samples studied here.

This assignment is also reinforced by some reported observations of surface mode located around 490 cm^{-1} in one dimensional ZnO nanostructures,[18–20] all close to the value we found. Moreover, our results show that TSO modes in a cylinder occur in a considerable different range of frequencies compared to SOP in nanospheres; these last are predicted by Fonoberov and Balandin[8] and observed by H. Zeng *et al.*[21] around 550 cm^{-1}. This point enlightens the role of the surface discontinuity in a cylinder.

Finally, we deal with the QC/SSO modes shown in Fig. 1(a). Considering nano-objects with an aspect ratio of unity, we can reasonably expect QC/SSO modes to occur with the same wave vector as TSO modes we observed, i.e., $aq_z \simeq q_r l/2=0.2$. According to Fig. 1(a), such a mode is in the QC spectral region no matter the value of ε_D. Thus, we do not expect to observe SSO modes, which is experimentally confirmed except to TSO mode; no mode located in the spectral range of SSO modes ($\omega \in [\omega_{\perp,TO};\omega_{\parallel,LO}]$) can be evidenced on the Raman spectra in Fig. 3. Of course, QC modes could be observed in the Raman spectra, but such modes are poor candidates to probe nano-object surface properties. In contrast, the observation of TSO modes is relevant and accurate enough to conclude about the specific localization of ligands around nano-objects. We also want to point out that calculations presented here can be easily tuned to predict SOP/IOP frequencies in wurtzite cylindrical NPs in solution or embedded in a solid matrix.

CONCLUSION

Surface modes in a cylinder of a wurtzite crystal have been calculated and their dispersion as a function of wave vector and dielectric constant of the outer medium has been discussed. Comparison with experimental data allows us to assign the strong peak in the Raman spectra to a symmetric top surface mode. The insensitivity of the frequency of this peak to the presence and diversity of ligands confirms that they are not coordinated to top surfaces of ZnO NPs but rather on their lateral surface.

[1] J.-Y. Marzin, J.-M. Gérard, A. Izraël, D. Barrier, and G. Bastard, Phys. Rev. Lett. **73**, 716 (1994).
[2] A. K. Sood, J. Menéndez, M. Cardona, and K. Ploog, Phys. Rev. Lett. **54**, 2115 (1985).
[3] L. Zhang and J. J. Shi, Semicond. Sci. Technol. **20**, 592 (2005).
[4] W. S. Li and C. Y. Chen, Physica B **229**, 375 (1997).
[5] K. W. Adu, Q. Xiong, H. R. Guiterrez, G. Chen, and P. C. Eklund, Appl. Phys. A: Mater. Sci. Process. **85**, 287 (2006).
[6] Ü. Ozgür, Ya. I. Alivov, C. Liu, A. Teke, M. A. Reshchikov, S. Dogan, V. Avrutin, S.-J. Cho, and H. Morkoç, J. Appl. Phys. **98**, 041301 (2005).
[7] C. Jagadish and S. J. Pearton, *Zinc Oxide Bulk, Thin Films and Nanostructures* (Elsevier, Amsterdam, 2006), Vol. 1, p. 15.
[8] V. A. Fonoberov and A. A. Balandin, Phys. Rev. B **70**, 233205 (2004).
[9] V. A. Fonoberov and A. Balandin, Phys. Status Solidi C **1**, 2650 (2005).
[10] V. A. Fonoberov and A. Balandin, J. Phys.: Condens. Matter **17**, 1085 (2005).
[11] M. Monge, M. L. Kahn, A. Maisonnat, and B. Chaudret, Angew. Chem., Int. Ed. **42**, 5321 (2003).
[12] K. A. Alim, V. A. Fonoberov, M. Shamsa, and A. A. Balandin, J. Appl. Phys. **97**, 124313 (2005).
[13] M. L. Kahn, T. Cardinal, B. Bousquet, M. Monge, V. Jubera, and B. Chaudret, ChemPhysChem **7**, 2362 (2006).
[14] R. Loudon, Adv. Phys. **13**, 423 (1964).
[15] C. A. Arguello, D. L. Rousseau, and S. P. S. Porto, Phys. Rev. **181**, 1351 (1969).
[16] Q. Xiong, J. Wang, O. Reese, L. C. Lew Yan Voon, and P. C. Eklund, Nano Lett. **4**, 1991 (2004).
[17] P.-M. Chassaing, F. Demangeot, V. Paillard, A. Zwick, N. Combe, C. Pagès, M. L. Kahn, A. Maisonnat, and B. Chaudret, Appl. Phys. Lett. **91**, 053108 (2007).
[18] V. V. Ursaki, M. Tiginyanu, V. V. Zalamai, V. M. Masalov, E. N. Samarov, G. A. Emelchenko, and F. Briones, J. Appl. Phys. **90**, 1001 (2004).
[19] B. Cheng, Y. Xiao, G. Wu, and L. Zhang, Appl. Phys. Lett. **84**, 416 (2004).
[20] V. Gupta, P. Bhattacharya, Y. I. Yuzuk, K. Streenivas, and R. S. Katiyar, J. Cryst. Growth **287**, 39 (2006).
[21] H. Zeng, W. Cai, B. Cao, J. Hu, Y. Li, and P. Liu, Appl. Phys. Lett. **88**, 181905 (2006).